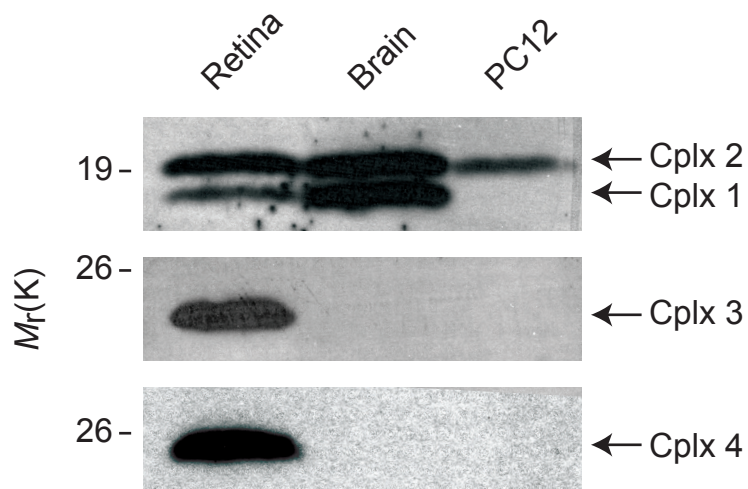


Real-time visualization of complexin during single exocytic events

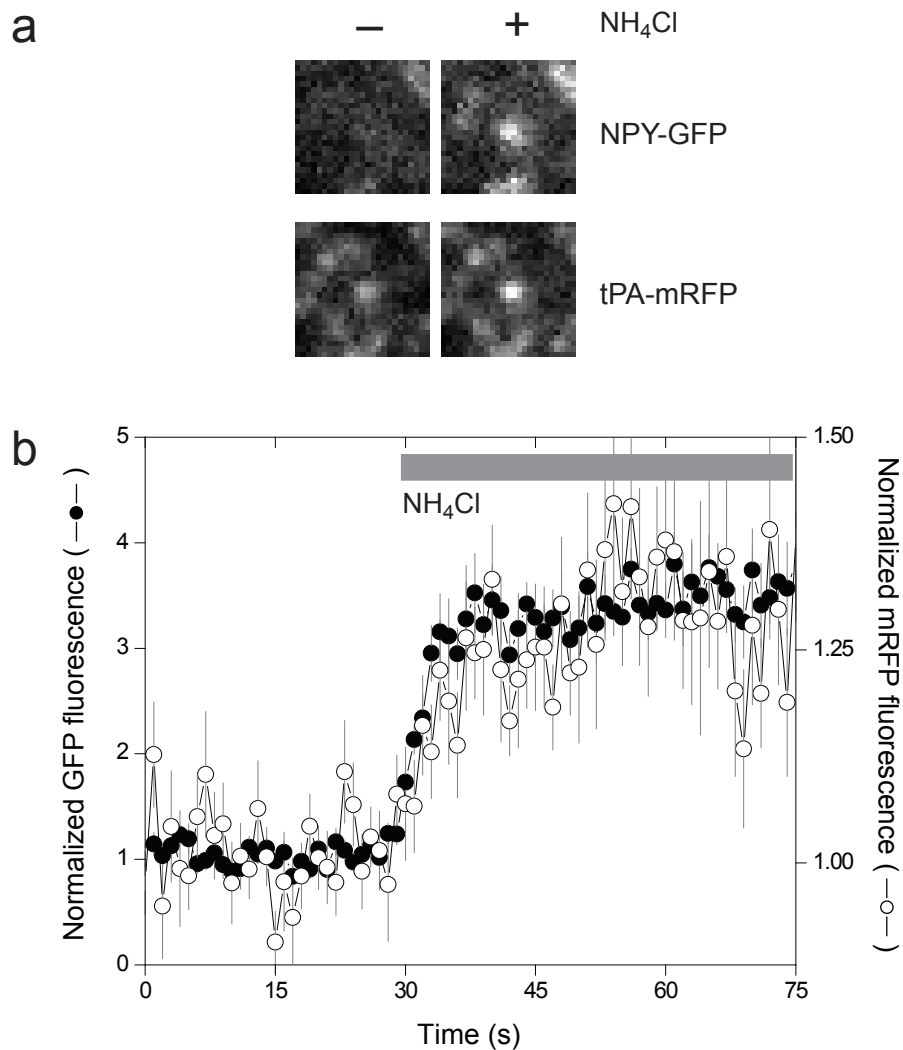
Seong J. An, Chad P. Grabner, David Zenisek

Supplementary Information

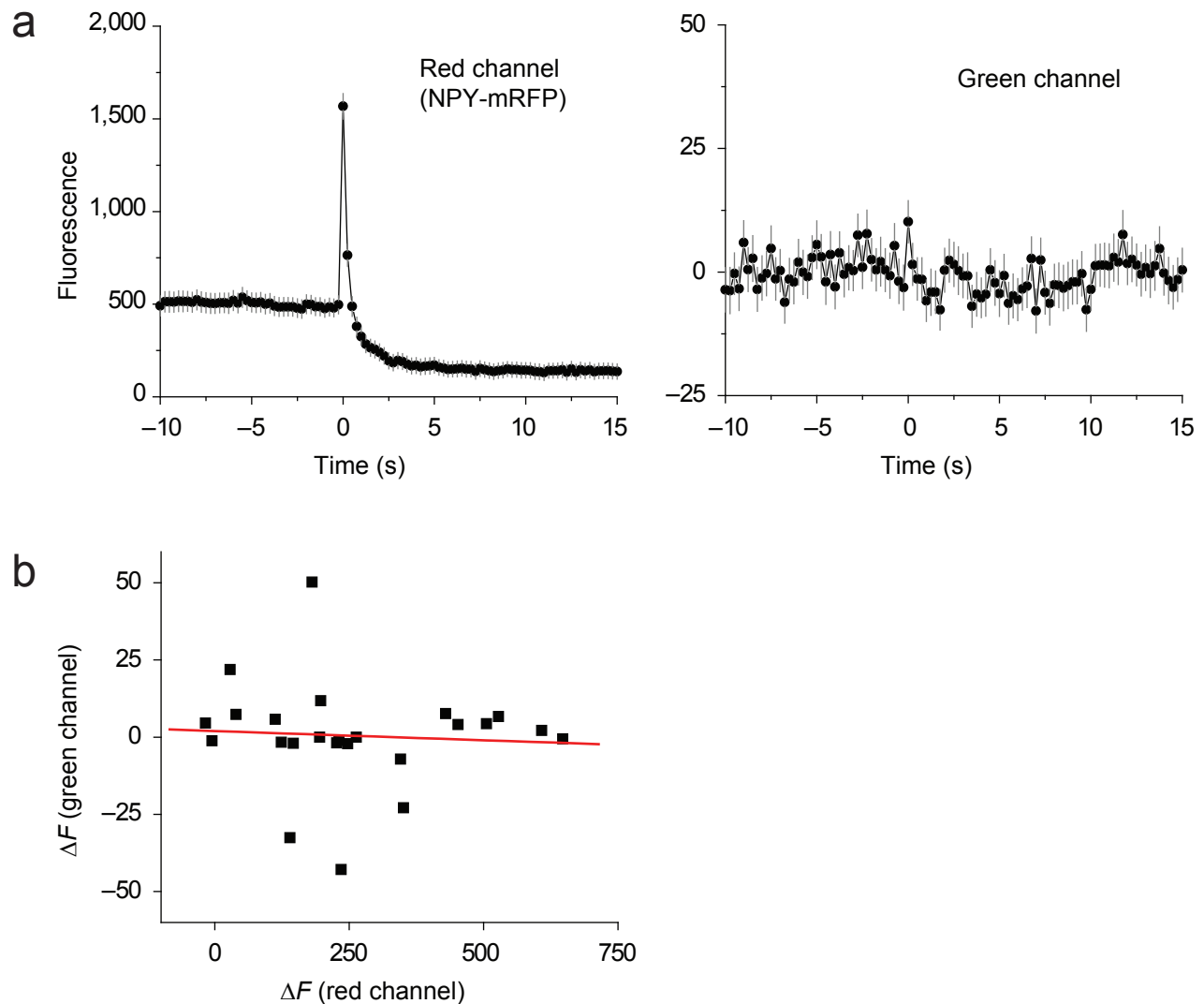
Supplementary Figures 1–16



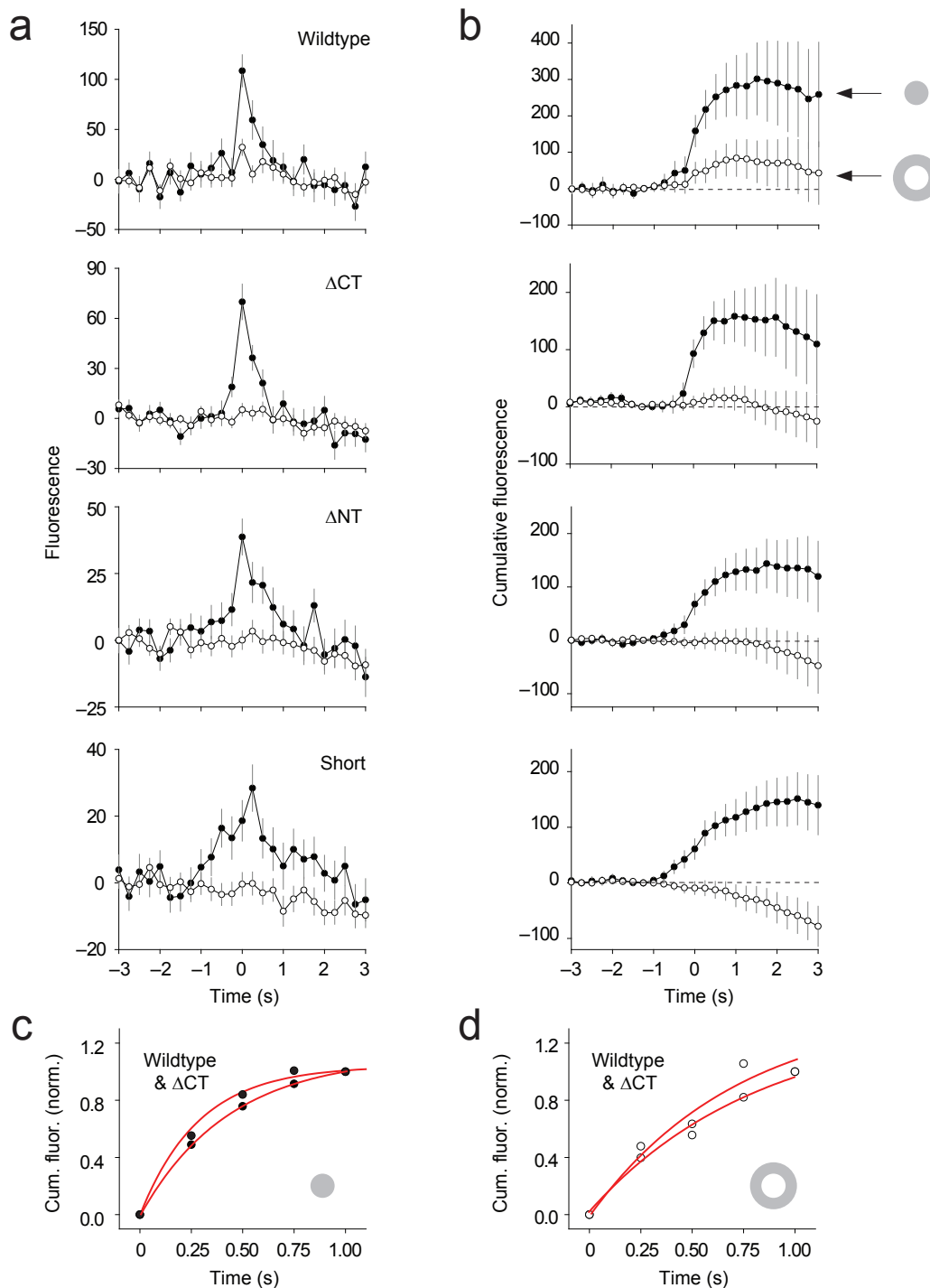
Supplementary Figure 1 PC12 cells endogenously express cplx 2. Homogenates of retina, brain and PC12 cells were immunoblotted for the indicated proteins. Note that cplx isoforms 1 and 2 are distinguished by their slightly different electrophoretic mobilities⁹.



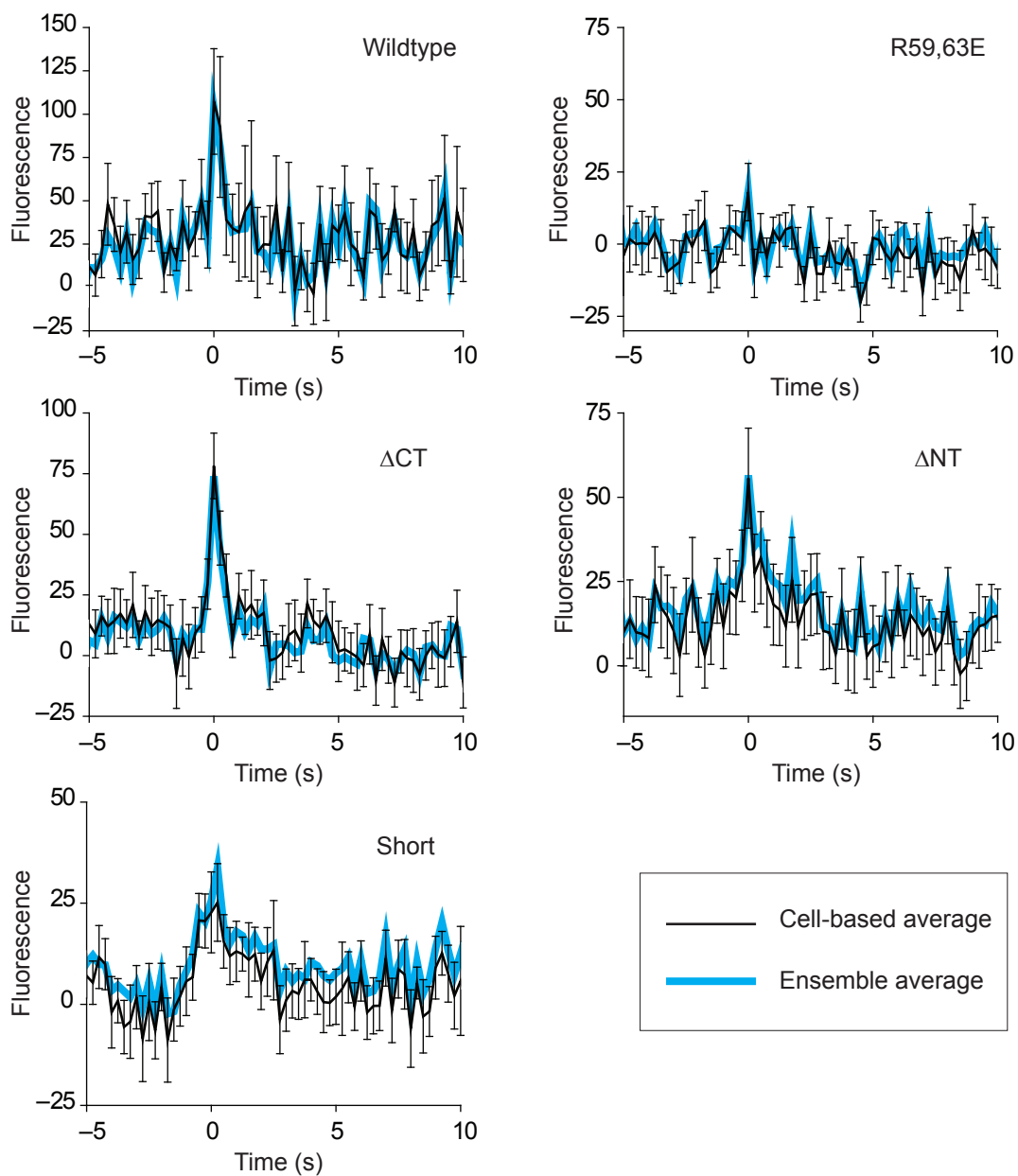
Supplementary Figure 2 Ammonium chloride-induced changes in granule fluorescence. **(a)** Images of a granule containing both GFP and mRFP, fused to either NPY or tissue plasminogen activator (tPA; see later) before and after external application of 50 mM ammonium chloride, which neutralizes the acidic pH of granules. **(b)** Fluorescence increase of GFP (closed circles; left ordinate) and mRFP (open circles; right ordinate) over time ($n = 9$ granules). Error bars are \pm s.e.m.



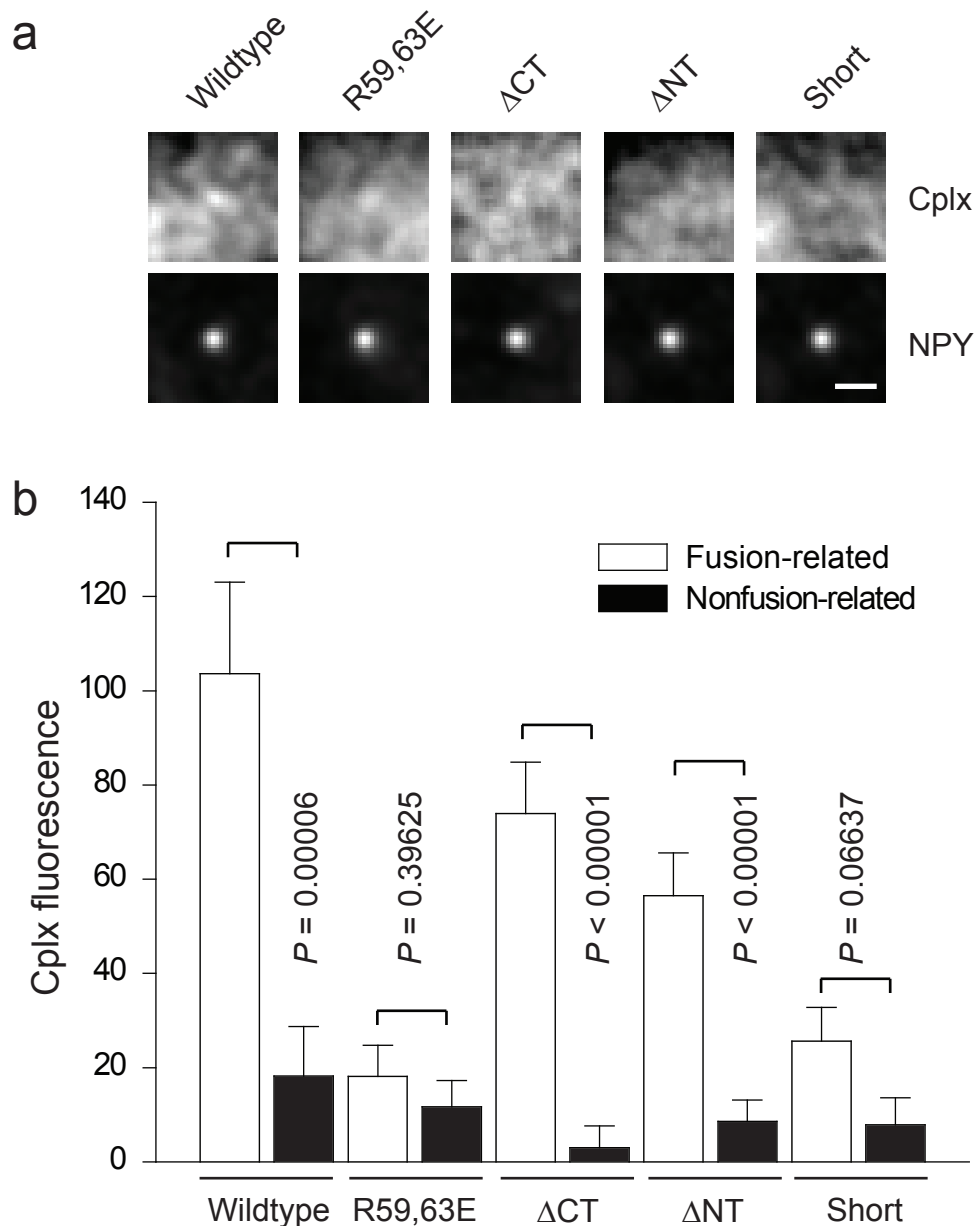
Supplementary Figure 3 Spectral bleedthrough of mRFP fluorescence is negligible. (a) Background-subtracted fluorescence of NPY-mRFP granules ($n = 480$) undergoing exocytosis and the fluorescence at the corresponding coordinates in the green channel. The average intensity of 50 frames after fusion (>0 s) was subtracted from that of 50 frames before fusion (<0 s) to obtain ΔF and relate fluorescence in the two channels. Green ΔF was 0.52% of red ΔF ; however, this 'green' fluorescence is the sum of two unknown quantities: mRFP fluorescence bypassing optical filters and autofluorescence of granules. (b) Correlation plot of red and green ΔF values. Each point is the average ΔF of all events from a single coverslip. The lack of a positive correlation (red line) suggests that fluorescence in the green channel does not represent bleedthrough. This is reasonable given the dissimilarity of the traces in a.



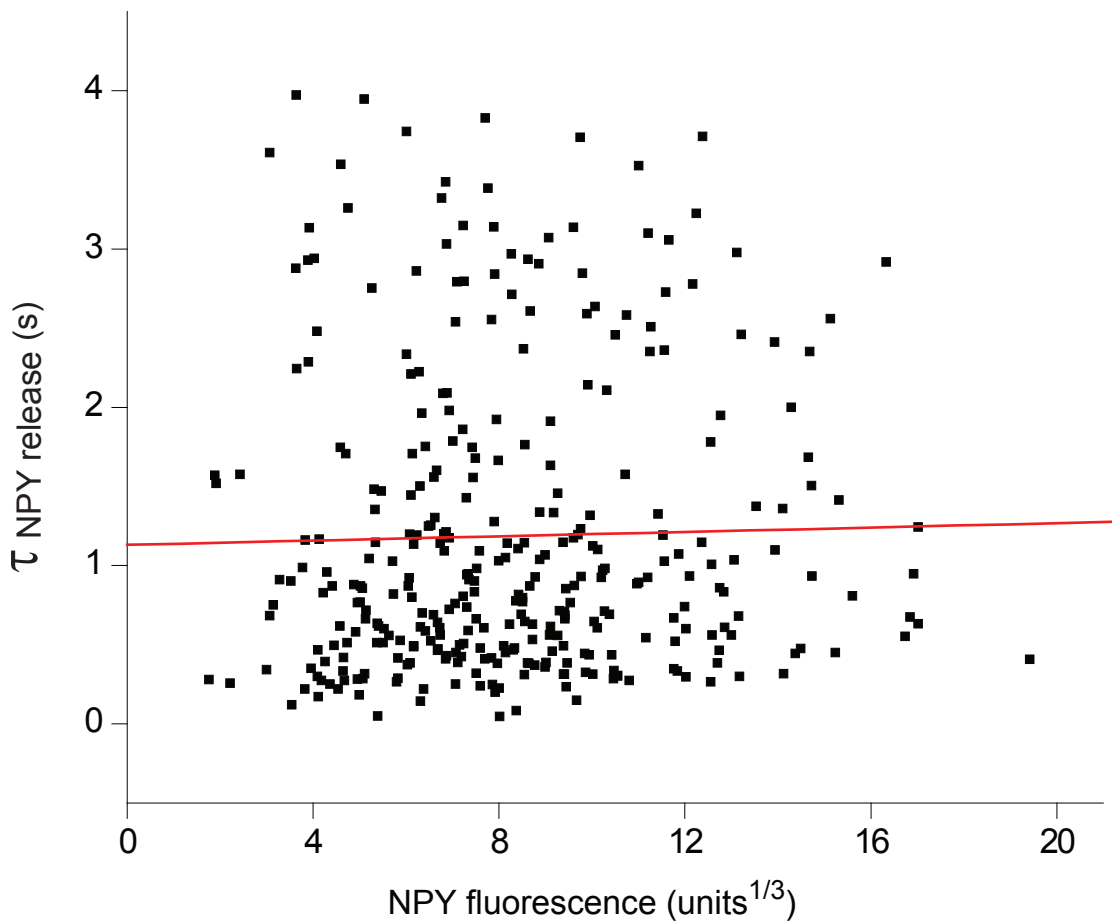
Supplementary Figure 4 Lateral spread of wildtype cplx-GFP and Δ CT-GFP fluorescence. **(a)** The average fluorescence of cplx-GFP signals within a 1.2- μ m-diameter circle (solid circles) and a concentric 1.3- μ m wide annulus (open circles). Time is relative to the moment of fusion. **(b)** Time integrals of **a** plotted to remove high-frequency noise. **(c)** Fluorescence in circular region of interest in **b** for wildtype cplx-GFP and Δ CT-GFP normalized to the cumulative intensity 1 s after fusion. **(d)** As in **c** but for annular fluorescence. Red lines, exponential fits. The slower fluorescence rise in the annulus ($\tau \sim 0.8$ s versus ~ 0.4 s) is consistent with the lateral spread of wildtype cplx-GFP and Δ CT-GFP from the center circle. Due to their dimmer signals, it is unclear if Δ NT-GFP and cplx short-GFP spread during fusion.



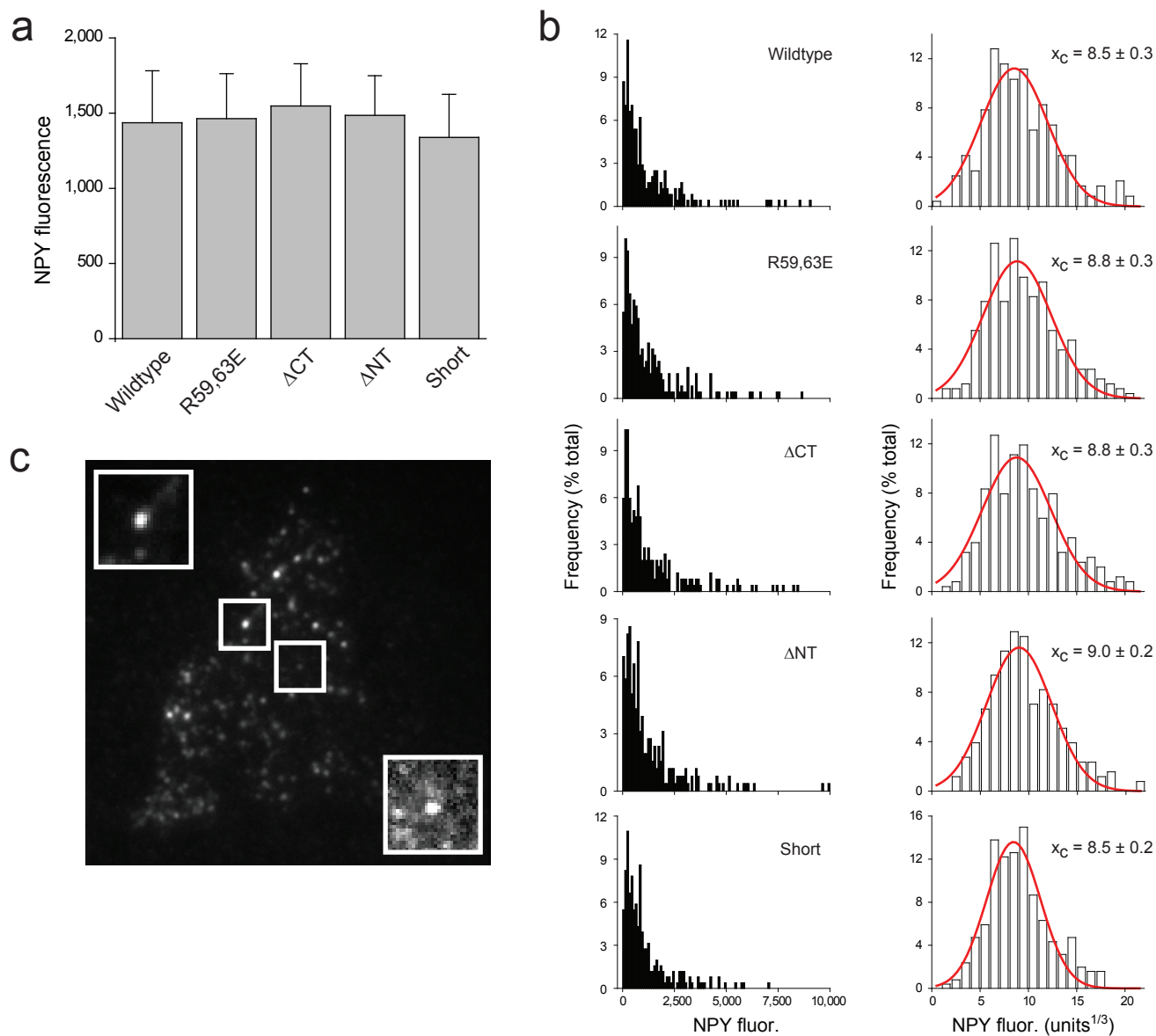
Supplementary Figure 5 Ensemble versus cell-based averages of cplx-GFP signals. Individual cell averages of cplx-GFP signals were averaged (\pm s.e.m) and overlaid on ensemble averages (thick cyan trace), which were replotted from **Figure 1a–e**. Details of the datasets are described in **Figure 1**.



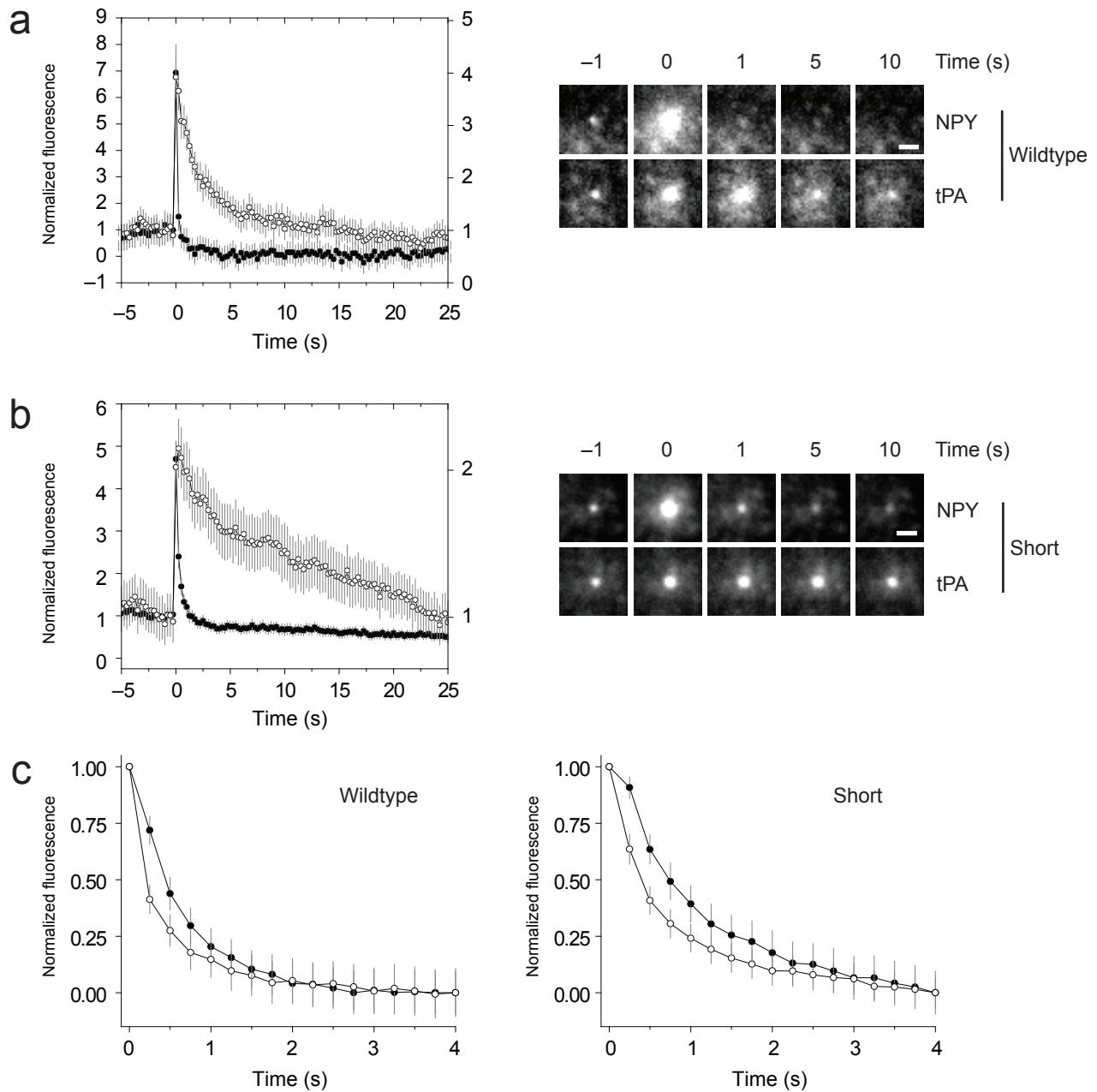
Supplementary Figure 6 Cplx-GFP signals at nonfusing granules. **(a)** Average images of cplx-GFP and nonfusing granules ($n = 256$ for each cplx construct). Granules that did not undergo exocytosis in cells analyzed in **Figure 1** were marked, and 10 successive frames before stimulation were averaged; the same was done for the corresponding coordinates in the cplx-GFP channel. Images were 3-pixel, low-pass filtered for clarity. Scale bar, 1 μ m. Note that the image of R59,63E-GFP is not visibly distinct from those of other cplx constructs. **(b)** Background-subtracted intensities of cplx-GFP in **a** (solid bars) and at $t = 0$ s in **Figure 1**, when granules undergo fusion (open bars). Error bars are \pm s.e.m. P values determined using a Student's t -test.



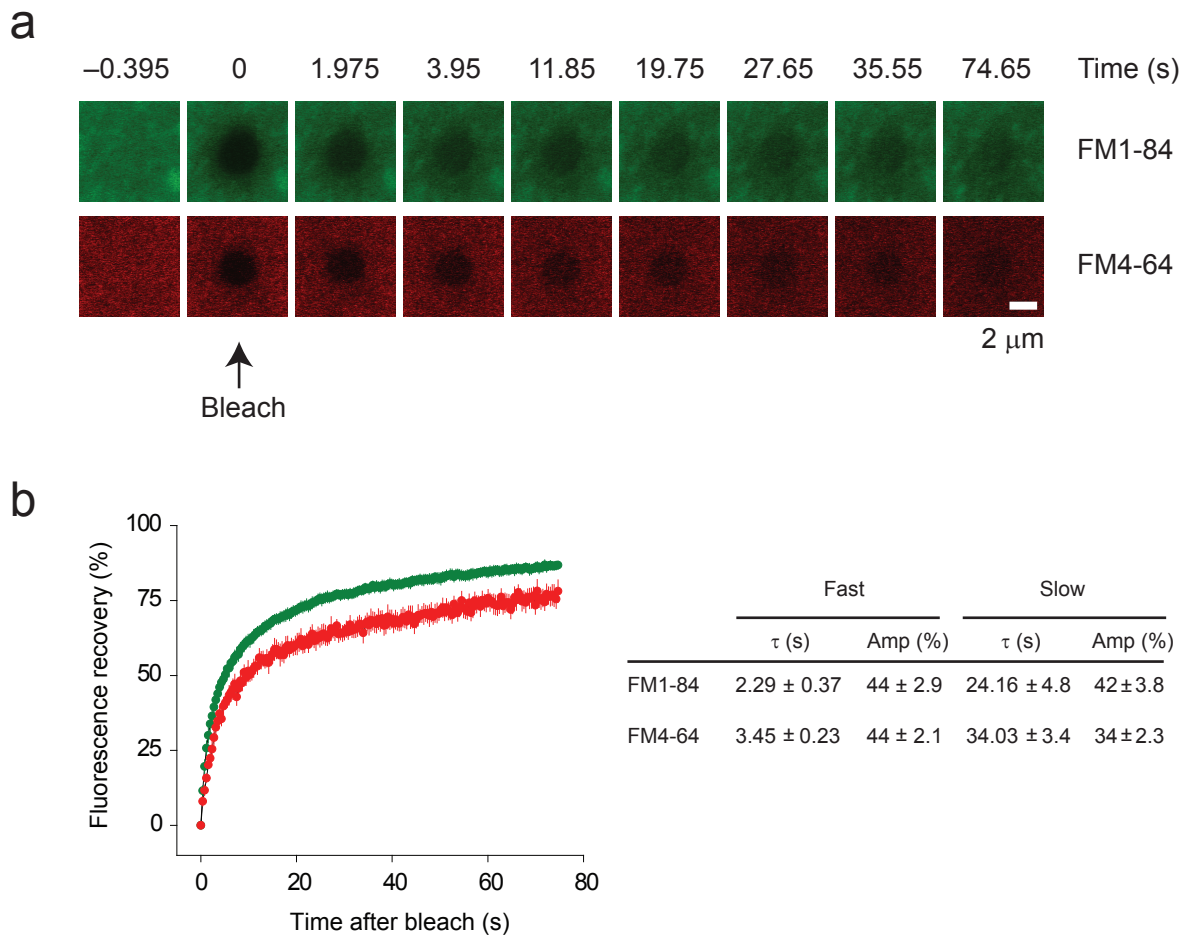
Supplementary Figure 7 Lack of correlation between NPY-mRFP release rate and granule intensity. Plot of NPY-mRFP release rates measured using the outer-circle fluorescence analysis described in **Figure 3a** versus the NPY-mRFP fluorescence of granules ($n = 336$). The cube root of granule fluorescence was used since granule intensities were broadly spread (see **Supplementary Fig. 8**). Data were collected from cells expressing only endogenous cplx.



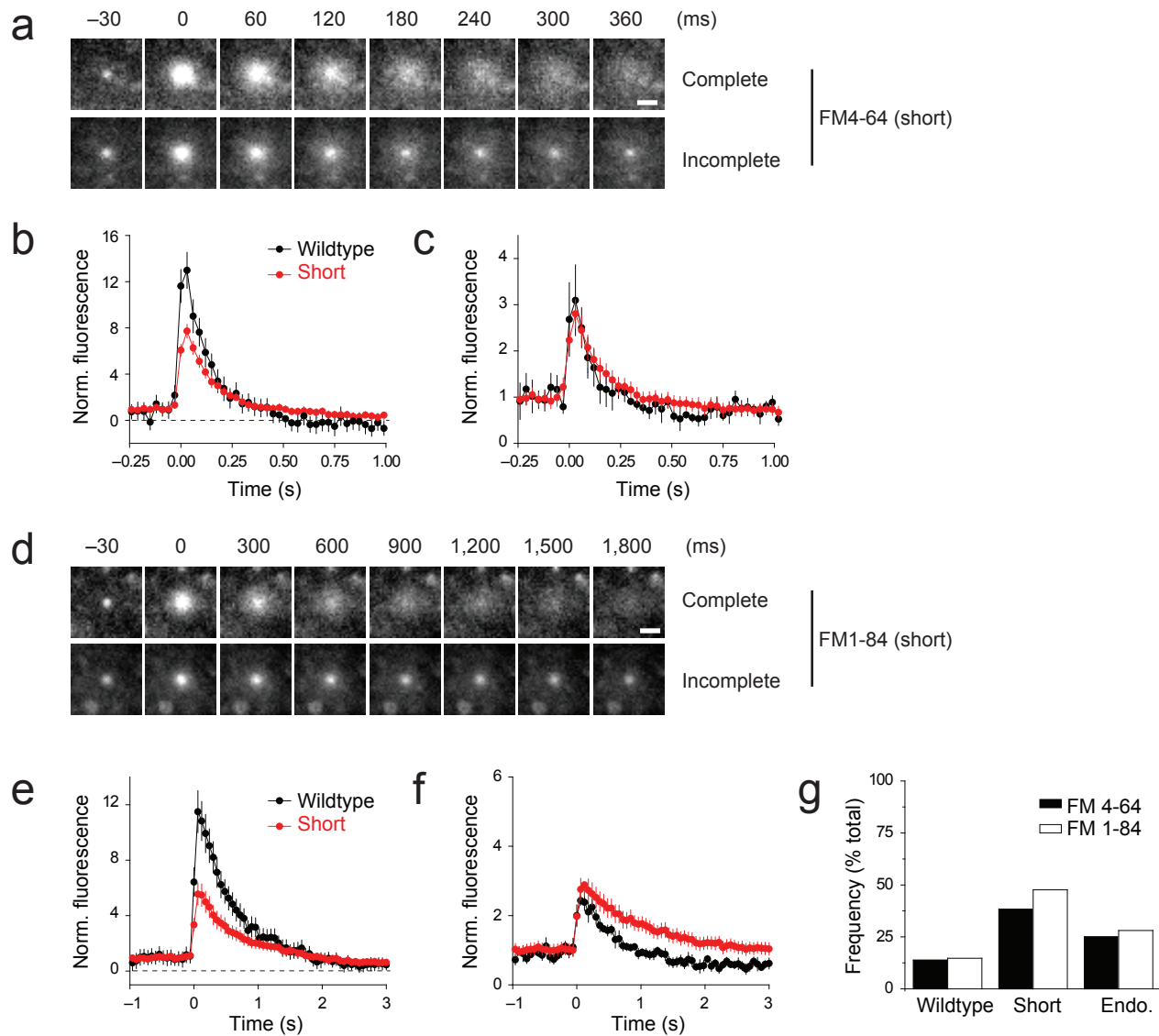
Supplementary Figure 8 Cplx expression does not affect loading of NPY-mRFP into granules. **(a)** Average NPY-mRFP fluorescence of nonfusing granules from the dataset in **Supplementary Figure 6** ($n = 256$ for each cplx construct). Error bars are \pm s.e.m. **(b)** Histogram of NPY-mRFP fluorescence of nonfusing granules (left) and that of the cube root of the fluorescence (right), fitted with Gaussians (red lines; x_c , peak center). The single Gaussian fits suggest a single population of granule sizes, since the amount of stored NPY-mRFP should vary with the cube of the granule diameter. **(c)** Representative footprint of NPY-mRFP-containing granules. This cell also coexpressed wildtype cplx-GFP (not shown). For clarity, the expanded image of the dimmer granule is shown at a different contrast setting. Square insets are $9 \mu\text{m}^2$.



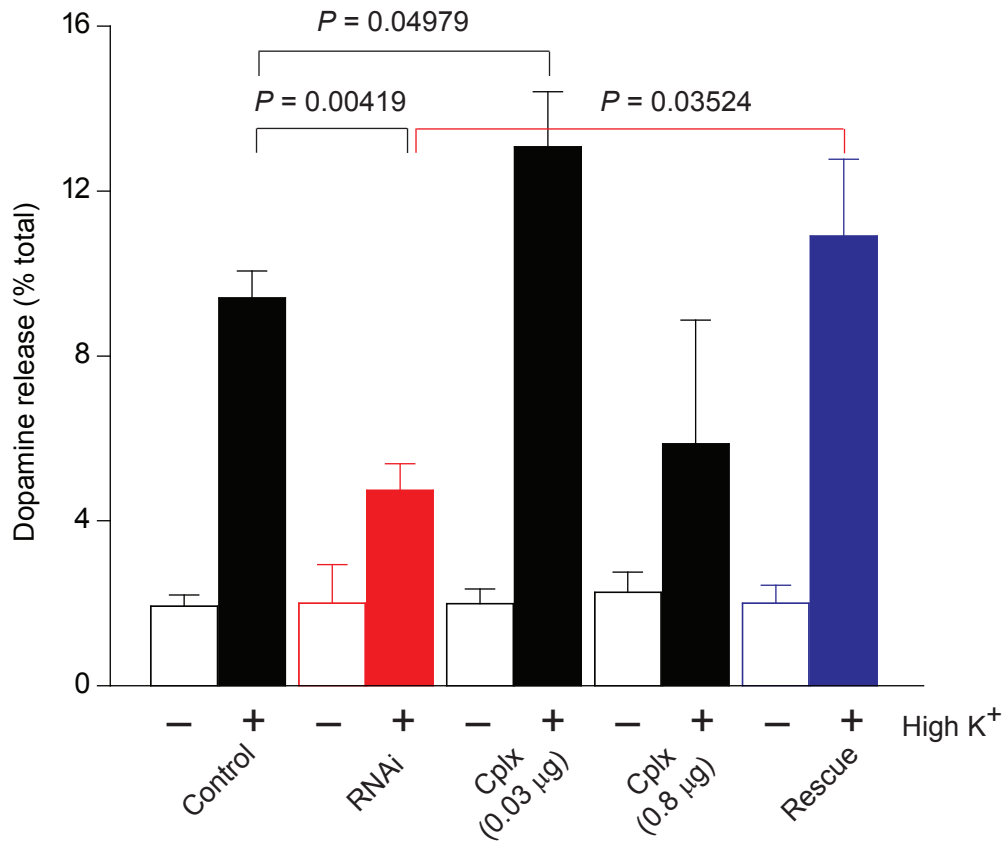
Supplementary Figure 9 Co-release of NPY-GFP and tPA-mRFP. **(a)** (Right) Averaged image sequence of granules ($n = 42$) co-releasing NPY-GFP and tPA-mRFP in cells transfected with wildtype cplx-GFP. To distinguish granules in the green channel, we selected cells with low cplx-GFP expression, which appeared as diffuse fluorescence throughout the footprint of the cell. This elevated fluorescence is not noticeable in the images, but it is obvious at different contrast settings. (Left) Background-subtracted fluorescence of NPY-GFP and tPA-mRFP at granule sites. Right and left ordinate, tPA-mRFP and NPY-GFP fluorescence, respectively, normalized to pre-fusion intensity. Because of the presence of wildtype cplx-GFP, the NPY-GFP trace overestimates the background fluorescence. **(b)** As in **a** but for cells transfected with cplx short-GFP ($n = 65$). **(c)** Lack of tPA influence on NPY release. Outer-circle NPY-GFP fluorescence of the events in **a** and **b**, averaged and normalized to initial-fusion intensity (open circles) and, for comparison, those of NPY-mRFP in the absence of tPA (solid circles, redrawn from **Fig. 3c**). The faster decline of the open circles in both plots is likely due to the artificial elevation of baseline fluorescence by cplx-GFP.



Supplementary Figure 10 Diffusion coefficients of FM dyes. **(a)** Fluorescence recovery after photobleaching (FRAP) of FM4-64 ($n = 7$) and FM1-84 ($n = 7$) on PC12 cells. Arrow indicates when a circular area $\sim 4.5 \mu\text{m}$ in diameter was bleached on the portion of the plasma membrane adhered to the coverslip. **(b)** FM4-64 (red) and FM1-84 (green) FRAP curves were fitted with two exponentials. Fast components yielded diffusion coefficients of 0.54 and $0.81 \mu\text{m}^2/\text{s}$ for FM4-64 and FM1-84, respectively, and are likely related to the lateral mobility of the dyes.

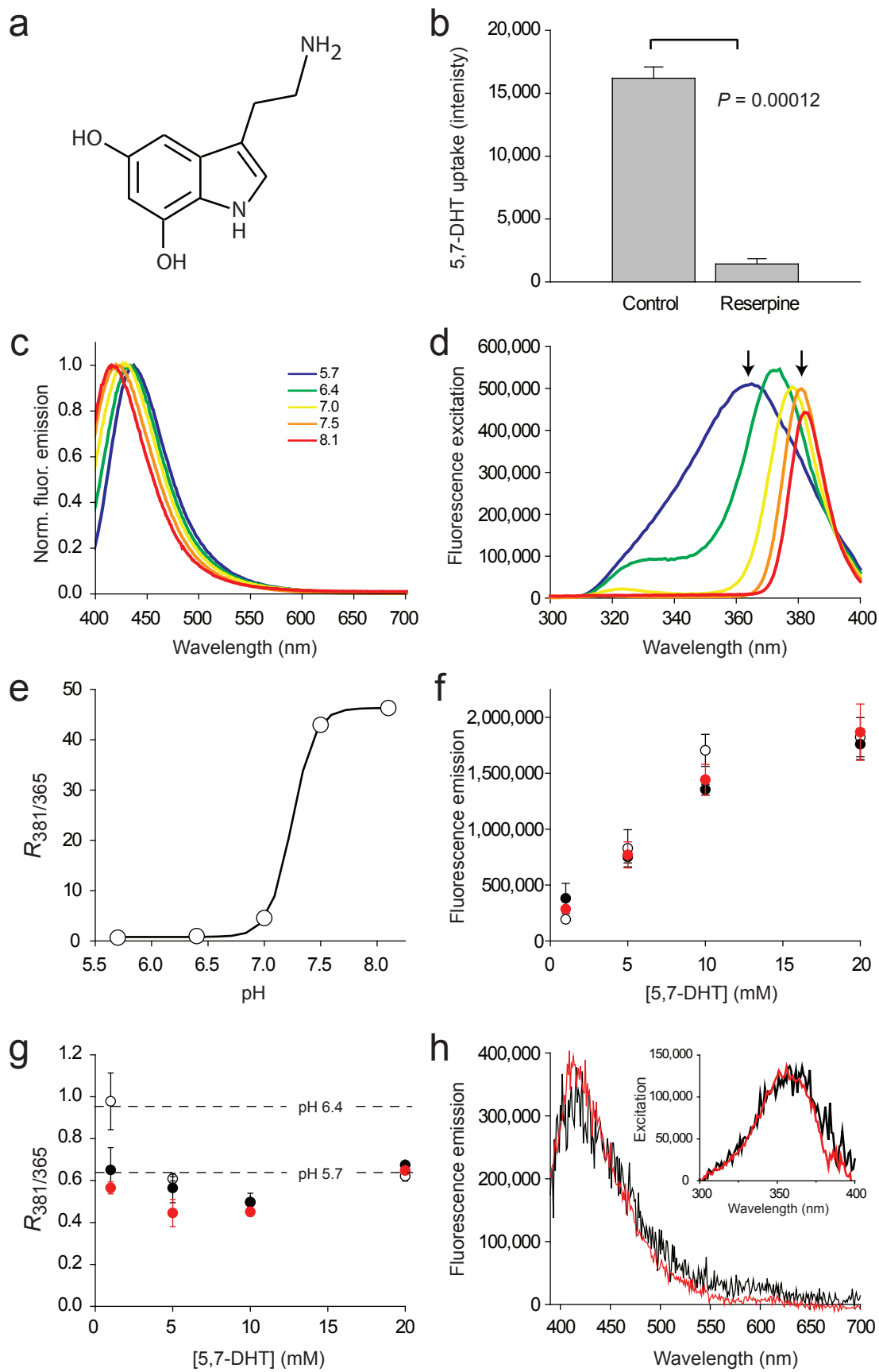


Supplementary Figure 11 Complete and incomplete release of FM dyes. **(a)** Averaged image sequence of granules releasing FM4-64 completely or incompletely from the cplx short-GFP dataset. **(b)** Background-subtracted fluorescence of complete FM4-64 release events with wildtype cplx-GFP (black, $n = 32$ events) or cplx short-GFP (red, $n = 48$ events), normalized to pre-fusion intensity. **(c)** Background-subtracted fluorescence of incomplete FM4-64 release events with wildtype cplx-GFP (black, $n = 5$ events) or cplx short-GFP (red, $n = 30$ events), normalized to pre-fusion intensity. **(d)** Averaged image sequence of granules releasing FM1-84 completely or incompletely from the cplx short-mRFP dataset. **(e)** Background-subtracted fluorescence of complete FM1-84 release events with wildtype cplx-mRFP (black, $n = 29$ events) or cplx short-mRFP (red, $n = 55$ events), normalized to pre-fusion intensity. **(f)** Background-subtracted fluorescence of incomplete FM1-84 release events with wildtype cplx-mRFP (black, $n = 5$ events) or cplx short-mRFP (red, $n = 50$ events), normalized to pre-fusion intensity. **(g)** Frequency of incomplete release of FM4-64 (solid bars) and FM1-84 (open bars) in cells expressing wildtype cplx, cplx short or only endogenous cplx. Note the similarity to the frequency of resealing events in **Figure 4c**.

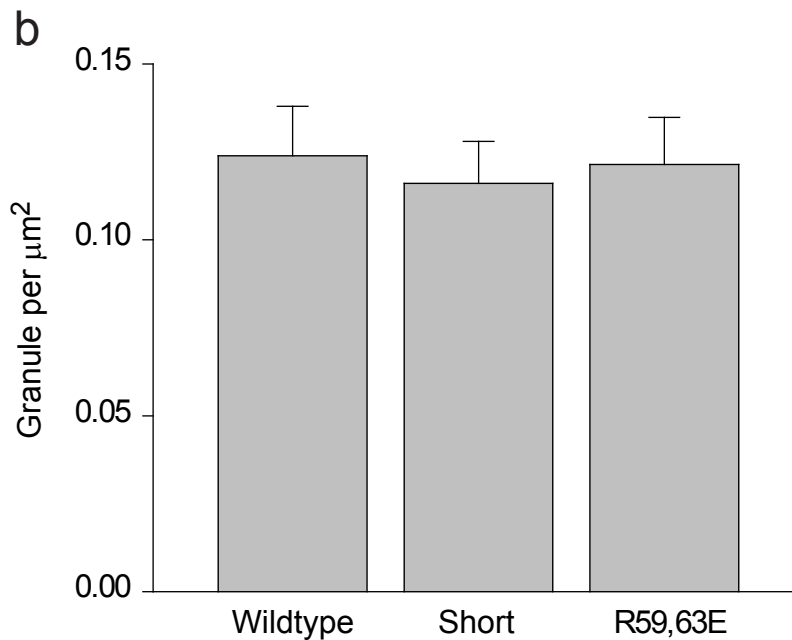
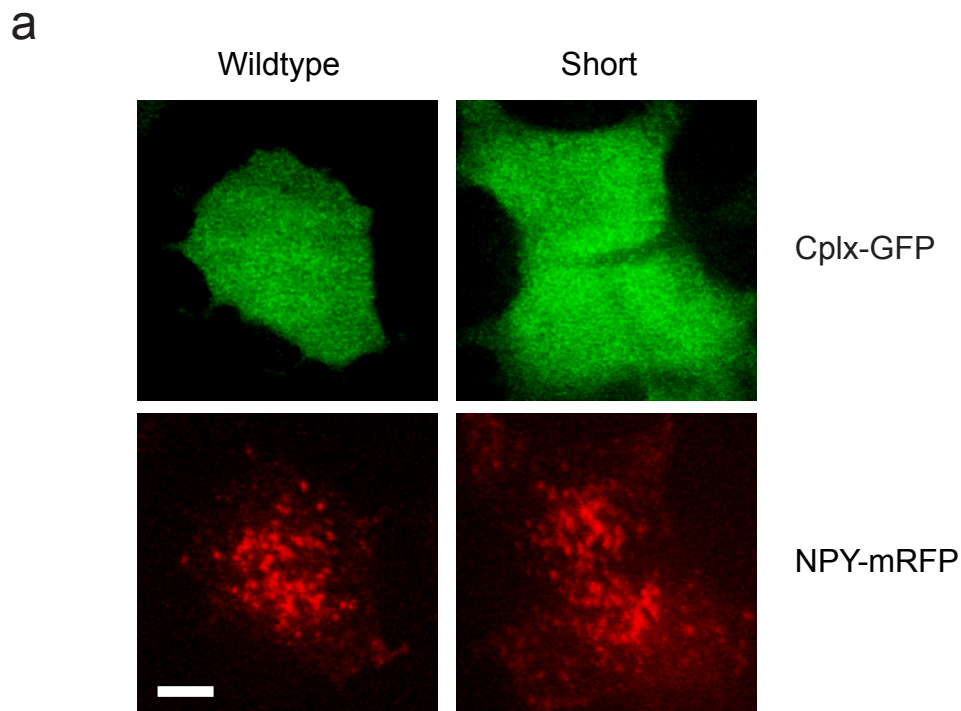


Supplementary Figure 12 Effects of cplx expression on dopamine release. Cells were incubated with dopamine (1 mM) in the presence of ascorbic acid (1 mM) for 60 min at 37°C. The cells were washed and incubated with low or high [K⁺] for 5 min. Released and total cellular dopamine were detected using an enzyme-linked immunosorbent assay. The data shown (mean ± s.e.m) are from four independent experiments. Cells were transfected with 0.03 µg of GFP plasmid (control), 1 µg shRNA (RNAi), 0.03 or 0.8 µg cplx-GFP, or 1 µg shRNA and 0.1 µg cplx-GFP plasmids (rescue). Note that the amounts of cplx-GFP plasmid were adjusted from those used in **Figure 6b** to offset the omission of NPY-mRFP plasmid in these transfections.

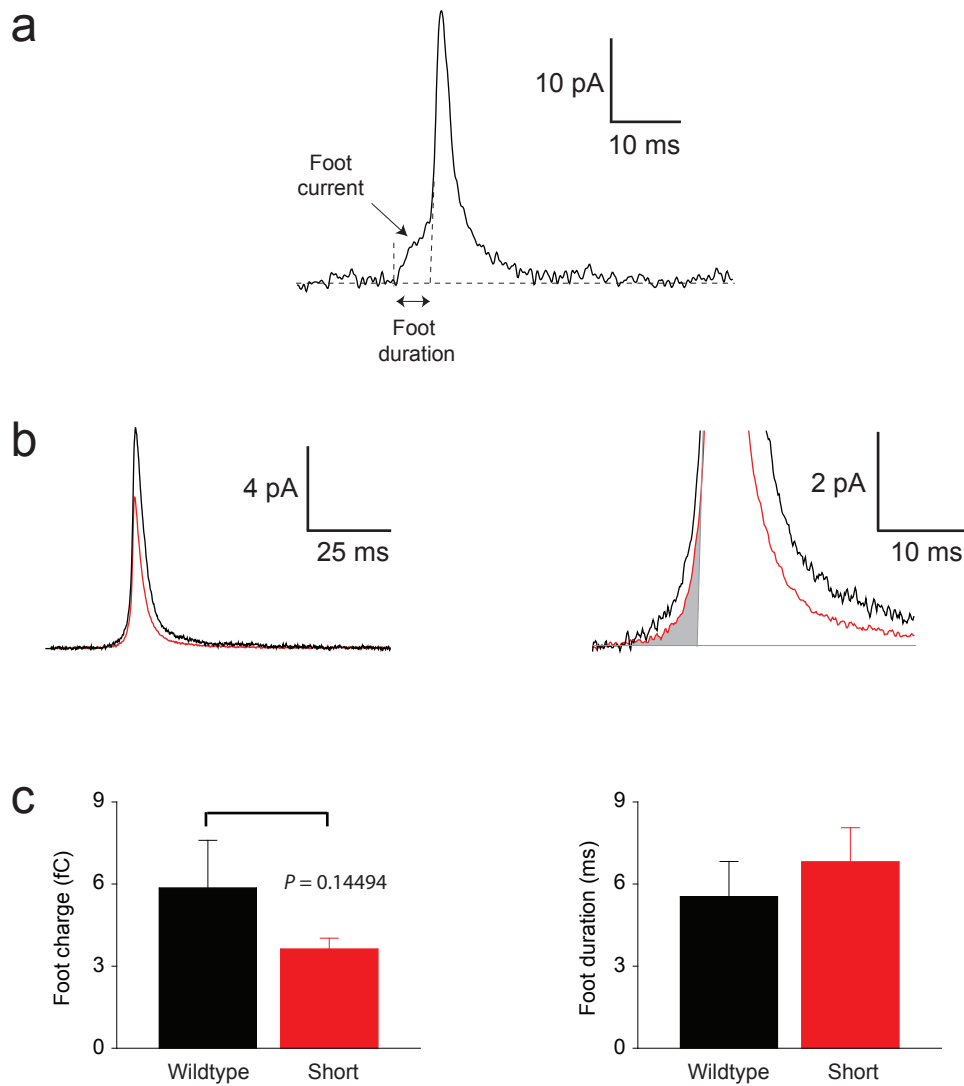
Supplementary Figure 13



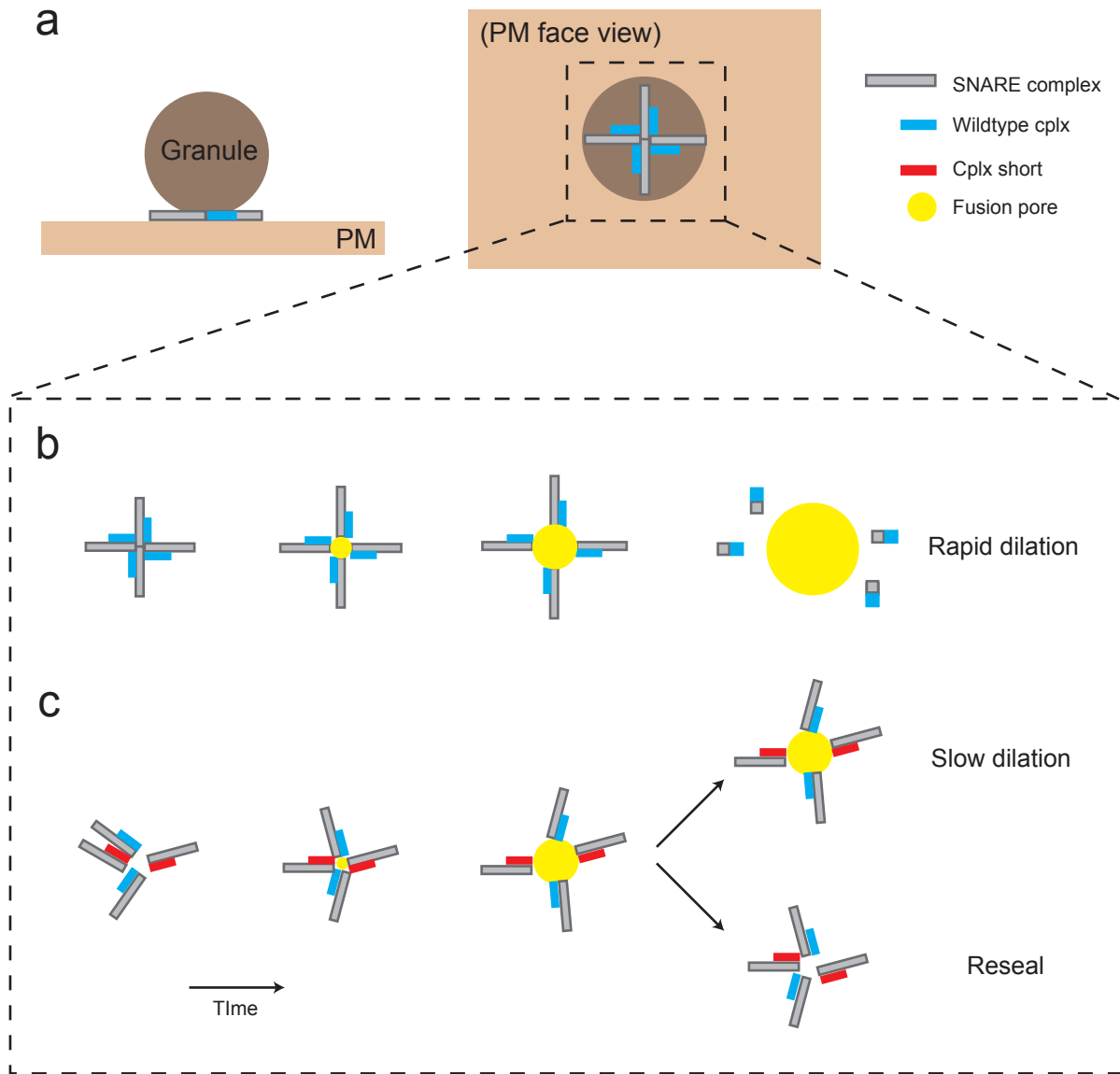
Supplementary Figure 13 Cplx expression does not affect loading of 5,7-DHT into granules. **(a)** Chemical structure of 5,7-DHT. **(b)** Inhibition of 5,7-DHT uptake by reserpine, a specific inhibitor of vesicular monoamine transporters. PC12 cells were incubated with 100 μ M 5,7-DHT at 37°C for 1 h in the presence or absence of 10 μ M reserpine. After washing, the cells were lysed with 1% Triton X-100 and the fluorescence emission at 420 nm was measured (mean \pm s.e.m., $n = 3$, $P = 0.00012$). **(c–e)** Fluorescence of 5,7-DHT (2 mM) in solution at different pH values. **(c)** Normalized emission spectra (excitation = 380 nm). **(d)** Excitation spectra (emission = 420 nm). Arrows indicate peaks at 365 and 381 nm for pH 5.7 and 7.5 samples, respectively. **(e)** Calibration curve of 381/365-nm excitation ratio ($R_{381/365}$). **(f,g)** Fluorescence of 5,7-DHT in cells. Cells transfected with wildtype cplx-mRFP (black circles), cplx short-mRFP (red circles), or mRFP alone (open circles) were incubated with the indicated concentrations of 5,7-DHT for 2 h. **(f)** Emission intensity at 420 nm. **(g)** $R_{381/365}$ (mean \pm s.e.m., $n = 3$). Dashed lines refer to $R_{381/365}$ values from **e**. **(h)** Cells expressing wildtype cplx-mRFP (black) or cplx short-mRFP (red) were incubated with 5 mM 5,7-DHT and isolated by FACS, based on mRFP fluorescence. Emission and excitation (inset) spectra of 5,7-DHT within cells were normalized by the number of cells sorted ($\sim 0.9\text{--}1.1 \times 10^6$ cells). This result indicates that the background of untransfected cells in **f** and **g** did not minimize the observation of potential loading differences.



Supplementary Figure 14 Cplx expression does not affect the size of the granule population. **(a)** Confocal images of cells cotransfected with NPY-mRFP and wildtype cplx-GFP or cplx short-GFP. Scale bar, 10 μm . **(b)** Granule density in cells expressing wildtype cplx-GFP, cplx short-GFP or R59,63E-GFP. Five Z-sections closest to the coverslip for each cell were summed and the granules were counted (see Methods). Error bars are \pm s.e.m. ($n = 10$ cells).



Supplementary Figure 15 Foot signals of amperometric events above 3 pA. **(a)** Individual example of an event above 3 pA from a cell expressing wildtype cplx-GFP. **(b)** Averaged current spikes of events above 3 pA with wildtype cplx-GFP (black) or with cplx short-GFP (red) aligned to their rising phase at 50% amplitude. Expanded traces (right) show the foot signal (shaded region) that precedes the spike. **(c)** Average foot duration and charge for events above 3 pA with wildtype cplx-GFP and cplx short-GFP. Error bars are \pm s.e.m.



Supplementary Figure 16 Model of SNARE complex and complexin function. (a) Plasma-membrane (PM) face view used to diagram dynamics of SNARE complexes and complexin during exocytosis. (b) By binding to the membrane-proximal half of SNARE complexes^{10,11}, wildtype cplx facilitates fusion in two ways: it stabilizes the SNARE complexes and, through the synergistic action of its N- and C-terminal regions (not depicted), also spatially aligns them. This ensures rapid fusion pore opening and dilation, which leads to full fusion. (c) In contrast, cplx short binds SNARE complexes, stabilizing them, but interferes with the coordinated action of wildtype cplx. This delays fusion. Once formed, the fusion pore continues to dilate slowly or reseals.